(Received 17 September 2025, Accepted 3 November 2025, Scheduled 9 November 2025)

Online Monitoring of Permanent-Magnet Flux in PMSM Based on Improved Adaptive Higher-Order Square-Root Cubature Kalman Flux-Linkage Observer

Junqin Liu[1,*], Zhentong Wang[1], Tianle Li[1], Feng Deng[1], Lin Liu[1], Kaihui Zhao[2], and Xiangfei Li[2]

[1] *National Key Laboratory of Power Grid Disaster Prevention and Mitigation College of Electrical and Information Engineering Changsha University of Science and Technology, Changsha 410114, Hunan, China*
[2] *College of Transportation and Electrical Engineering, Hunan University of Technology, Zhuzhou 412007, China*

ABSTRACT: To enable accurate online observation of permanent-magnet (PM) flux linkage in permanent-magnet synchronous motors (PMSMs), this paper proposes an improved adaptive higher-order square-root cubature Kalman filter (IAHSRCKF) flux-linkage observer. Firstly, a nonlinear PMSM model is established to capture complex operating conditions. Secondly, fifth-order cubature integration and an adaptive estimator are embedded into a square-root cubature Kalman framework, yielding an adaptive fifth-order SRCKF observer that tracks PM flux-linkage variations under parameter drift and disturbances. Then, experimental scenarios are created by perturbing key electromagnetic and mechanical parameters and injecting external time-varying disturbances. Finally, simulation and hardware tests benchmark the proposed IAHSRCKF against UKF, CKF, and SRCKF. Results demonstrate that IAHSRCKF achieves the highest flux-estimation accuracy, exhibits low sensitivity to parameter uncertainties, and maintains strong robustness across complex operating conditions, thereby enabling reliable online monitoring of PM flux linkage.

1. INTRODUCTION

Permanent-magnet synchronous motors (PMSMs) are widely used in industrial drives, electric vehicles, and railway transportation owing to their excellent dynamic performance [1, 2]. However, during operation, the permanent-magnet material in a PMSM may undergo demagnetization due to factors such as temperature rise, mechanical vibration, and armature reaction [3, 4]. Demagnetization of the magnets or fluctuations in the magnetic field can directly cause abnormal heating and degraded torque performance; in severe cases, the motor may fail, which greatly limits the application of PM machines [5, 6]. To reduce the economic losses caused by PM demagnetization faults, it is therefore necessary to implement online monitoring of the motor's permanent magnets so as to lower maintenance costs [7, 8].

Regarding flux-linkage observation for PMSM, many scholars have conducted extensive research. In [9], a dual-adaptive unscented Kalman filter (UKF)-based observer was proposed to estimate the flux linkage, but the algorithm requires long iterative computation time, and its estimation accuracy is limited. Ref. [10] decouples the flux linkage from resistance by injecting a triangular-wave signal into the rotor position, and then constructs a flux observer for interior PMSM (IPMSM) using an extended Kalman filter (EKF); however, it does not address estimation accuracy under complex operating conditions. In [11], a predictive fault-tolerant control method based on online flux detection with an adaptive observer is presented, which computes state-current estimates by monitoring the real-time PM flux loss and feeds them back to the controller, but it cannot effectively handle the delay inherent to predictive control. Ref. [12] designs a nonsingular terminal sliding-mode observer to detect demagnetization; compared with conventional sliding-mode observers, it improves torque accuracy, yet relying on the observer alone cannot effectively cope with PMSM demagnetization faults. Ref. [13] developed an online permanent magnet flux monitoring method based on the EKF, which achieved satisfactory performance. However, the EKF introduces linearization errors due to the nonlinear nature of the PMSM model, potentially leading to filter instability. Moreover, it requires the computation of Jacobian matrices, which is computationally intensive and consumes significant microprocessor resources. Building on the work in [13], the authors of [14] integrated the Recursive Least Squares (RLS) algorithm with EKF to achieve step-by-step identification of motor parameters. This approach avoids the underdetermination of the identification model caused by parameter coupling. Additionally, the incorporation of the multi-innovation theory during the distributed identification process enhances data utilization.

In this paper, considering the variations in PMSM parameters and the coupling between external disturbances and flux linkage, we address the limitations of traditional Kalman Filter (KF) in terms of estimation accuracy under complex operat-

* Corresponding author: Junqin Liu (ljq2321925777@163.com).

ing conditions. The proposed approach aims to reduce inherent system delay while further mitigating linearization errors and computational burden, thereby enhancing the stability of the filter. This paper proposes an Improved Adaptive Higher-Order Square-Root Cubature Kalman Filter (IAHSRCKF) flux-linkage observation algorithm for PMSM. Firstly, a nonlinear mathematical model of the PMSM is established. Then, fifth-order cubature integration and an adaptive estimator are combined within a square-root cubature Kalman filter framework to construct an IAHSRCKF flux observer for real-time estimation of the PM flux linkage. By designing operating conditions with parameter perturbations and time-varying disturbances, simulations verify the algorithm's high flux-estimation accuracy and strong robustness, and experimental results further confirm the feasibility and effectiveness of the proposed method.

2. MATHEMATICAL MODEL OF PMSM

Neglecting all losses, the d-q-axis stator voltage equation of the PMSM is [15]:

$$\begin{cases} u_d = R_s i_d + L_d \frac{di_d}{dt} - \omega_e L_q i_q \\ u_q = R_s i_q + L_q \frac{di_q}{dt} + \omega_e \left(L_d i_d + \psi_f\right) \end{cases} \tag{1}$$

where i_d represents the stator d-axis current, i_q the stator q-axis current, u_d the stator d-axis voltage, u_q the stator q-axis voltage, ψ_f the permanent-magnet flux linkage, ω_e the electrical angular velocity, L_d the stator winding d-axis inductance, L_q the stator winding q-axis inductance, and R_s the stator resistance.

The electromagnetic torque equation of the PMSM is:

$$T_e = \frac{3}{2} n_p \left[\psi_f + \left(L_d - L_q\right) i_d\right] i_q \tag{2}$$

where T_e represents the electromagnetic torque, and n_p represents the number of pole pairs.

The mechanical motion equation of the PMSM is:

$$\frac{d\omega_e}{dt} = \frac{n_p}{J}\left(T_e - T_L - B\omega_m\right) \tag{3}$$

where J represents the moment of inertia, T_L the load torque, B the viscous friction coefficient, and ω_m the mechanical angular velocity.

In practical engineering applications, due to factors such as temperature, mechanical stress, and other influences, the electromagnetic parameters of PMSM (such as resistance, inductance, and flux linkage) as well as mechanical parameters (such as moment of inertia and damping coefficient) undergo nonlinear time-varying perturbations. Moreover, PMSM is also subjected to external time-varying disturbances and other factors in the actual operating environment. These uncertainties and "disturbances" significantly affect the motor's performance, influencing its dynamic behavior and stability. Therefore, the parameter variation equation of the PMSM under actual operating conditions is given by:

$$\begin{cases} \tilde{R}_s = R_s + \Delta R_s \\ \tilde{L}_d = L_d + \Delta L_d \\ \tilde{L}_q = L_q + \Delta L_q \\ \tilde{\psi}_f = \psi_f + \Delta\psi_f \\ \tilde{B} = B + \Delta B \\ \tilde{T}_L = T_L + \Delta T_L \\ \tilde{J} = J + \Delta J \end{cases} \tag{4}$$

where $\tilde{R}_s$, $\tilde{L}_d$, $\tilde{L}_q$, and $\tilde{\psi}_f$ represent the actual values of the electromagnetic parameters of the IPMSM under parameter perturbations and external time-varying disturbances; ΔR_s represents the stator phase resistance perturbation; ΔL_d represents the stator winding d-axis inductance perturbation; ΔL_q represents the stator winding q-axis inductance perturbation; $\Delta\psi_f$ represents the rotor flux linkage perturbation; $\tilde{B}$ and $\tilde{J}$ represent the actual values of the mechanical parameters of the PMSM under parameter perturbations; $\tilde{T}_L$ represents the actual load of the PMSM under time-varying operating conditions; ΔB represents the viscous friction coefficient perturbation; ΔJ represents the moment of inertia perturbation; ΔT_L represents the variation of the load torque.

Considering the parameter composite perturbations and external time-varying disturbance conditions, based on Eq. (1) to Eq. (4), the nonlinear mathematical equations of the PMSM can be rewritten as:

$$\begin{cases} u_d = \tilde{R}_s i_d + \frac{d\tilde{\psi}_d}{dt} - \omega_e \tilde{\psi}_q \\ u_q = \tilde{R}_s i_q + \frac{d\tilde{\psi}_q}{dt} + \omega_e \tilde{\psi}_d \\ T_e = \frac{3}{2} n_p \left[\tilde{\psi}_f + (\tilde{L}_d - \tilde{L}_q) i_d\right] i_q \\ \frac{d\omega_e}{dt} = \frac{n_p}{\tilde{J}}\left(T_e - \tilde{T}_L - \tilde{B}\omega_m\right) \end{cases} \tag{5}$$

Eq. (5) is rewritten as:

$$\begin{cases} \frac{di_d}{dt} = \frac{1}{\tilde{L}_d}\left(u_d + n_p \omega_m \tilde{L}_q i_q - \tilde{R}_s i_d\right) \\ \frac{di_q}{dt} = \frac{1}{\tilde{L}_q}\left(u_q - n_p \omega_m \tilde{L}_d i_d - n_p \omega_m \tilde{\psi}_f - \tilde{R}_s i_q\right) \\ \frac{\mathrm{d}\omega_m}{\mathrm{d}t} = \frac{1}{\tilde{J}}\left(T_e - \tilde{T}_L - \tilde{B}\omega_m\right) \\ \frac{d\tilde{\psi}_f}{dt} = \Delta\dot{\psi}_f \end{cases} \tag{6}$$

Selecting the state variables: $x^* = [\ i_d \quad i_q \quad \omega_m \quad \tilde{\psi}_f]^T$, $y = [\ i_d \quad i_q]^T$, $u = [\ u_d \quad u_q \quad T_e \quad \tilde{T}_L]^T$. Establishing the nonlinear mathematical model of the PMSM [16]:

$$\begin{cases} \dot{x}^*(t) = Ax(t) + Bu(t) + w \\ y(t) = Cx(t) + v \end{cases} \tag{7}$$

where $A = \begin{bmatrix} -\frac{\tilde{R}_s}{\tilde{L}_d} & \frac{\tilde{L}_q n_p \omega_m}{\tilde{L}_d} & 0 & 0 \\ -\frac{\tilde{L}_d n_p \omega_m}{\tilde{L}_q} & -\frac{\tilde{R}_s}{\tilde{L}_q} & -\frac{n_p \tilde{\psi}_f}{\tilde{L}_q} & 0 \\ 0 & 0 & -\frac{\tilde{B}}{\tilde{J}} & 0 \\ 0 & 0 & 0 & 0 \end{bmatrix}$; $C = \begin{bmatrix} 1 & 0 & 0 & 0 \\ 0 & 1 & 0 & 0 \end{bmatrix}$; $B = \begin{bmatrix} \frac{1}{\tilde{L}_d} & 0 & 0 & 0 \\ 0 & \frac{1}{\tilde{L}_q} & 0 & 0 \\ 0 & 0 & \frac{1}{\tilde{J}} & -\frac{1}{\tilde{J}} \\ 0 & 0 & 0 & 0 \end{bmatrix}$.

Discretizing the state equations and letting T be the sampling period:

$$\begin{cases} \dot{x}^*(k) = Gx(k-1) + Hu(k-1) + W_{k-1} \\ Y(k-1) = Cx(k-1) + v_{k-1} \end{cases} \tag{8}$$

where $G = \begin{bmatrix} 1 - \frac{\tilde{R}_s T}{\tilde{L}_d} & \frac{\tilde{L}_q n_p \omega_m T}{\tilde{L}_d} & 0 & 0 \\ -\frac{\tilde{L}_d n_p \omega_m T}{\tilde{L}_q} & 1 - \frac{\tilde{R}_s T}{\tilde{L}_q} & -\frac{n_p \tilde{\psi}_f T}{\tilde{L}_q} & 0 \\ 0 & 0 & 1 - \frac{\tilde{B} T}{\tilde{J}} & 0 \\ 0 & 0 & 0 & 1 \end{bmatrix}$; $C = \begin{bmatrix} 1 & 0 & 0 & 0 \\ 0 & 1 & 0 & 0 \end{bmatrix}$; $H = \begin{bmatrix} \frac{T}{\tilde{L}_d} & 0 & 0 & 0 \\ 0 & \frac{T}{\tilde{L}_q} & 0 & 0 \\ 0 & 0 & \frac{T}{\tilde{J}} & -\frac{T}{\tilde{J}} \\ 0 & 0 & 0 & 0 \end{bmatrix}$.

3. DESIGN OF IAHSRCKF FLUX-LINKAGE OBSERVER

Selecting the fifth-order cubature integration formula [16]:

$$\xi_i = \begin{cases} [0, \cdots, 0]^{\mathrm{T}} & i = 0 \\ \sqrt{n+2} \times \varepsilon_i^+ & i = 1, \cdots, \frac{n(n-1)}{2} \\ -\sqrt{n+2} \times \varepsilon^+_{i-\frac{n(n-1)}{2}} & i = \frac{n(n-1)}{2} + 1, \cdots, n(n-1) \\ \sqrt{n+2} \times \varepsilon^-_{i-n(n-1)} & i = n(n-1)+1, \cdots, \frac{3n(n-1)}{2} \\ -\sqrt{n+2} \times \varepsilon^-_{i-\frac{3n(n-1)}{2}} & i = \frac{3n(n-1)}{2} + 1, \cdots, 2n(n-1) \\ \sqrt{n+2} \times \mathrm{e}_{i-2n(n-1)} & i = 2n(n-1)+1, \cdots, n(2n-1) \\ -\sqrt{n+2} \times \mathrm{e}_{i-n(2n-1)} & i = n(2n-1)+1, \cdots, 2n^2 \end{cases} \tag{9}$$

where e_i is the n-dimensional unit vector, with its ith element equal to 1. The point sets $\{\varepsilon_j^+\}$ and $\{\varepsilon_j^-\}$ are:

$$\begin{cases} \varepsilon_j^+ \triangleq \sqrt{\frac{1}{2}} \times (e_k + e_l) : k < l \quad k, l = 1, \cdots, n \\ \varepsilon_j^- \triangleq \sqrt{\frac{1}{2}} \times (e_k - e_l) : k < l \quad k, l = 1, \cdots, n \end{cases} \tag{10}$$

The corresponding weight coefficient ω_i is:

$$\omega_i = \begin{cases} 2/(n+2) & i = 0 \\ 1/(n+2)^2 & i = 1, \cdots, 2n(n-1) \\ (4-n)/2(n+2)^2 & i = 2n(n-1), \cdots, 2n^2 \end{cases} \tag{11}$$

Based on the *Sage-Husa* recursive estimation method [17], design a time-varying noise statistical estimator to estimate the variance $\hat{R}_k$ of $v(k)$ online.

$$\hat{R}_k = (1 - d_{k-1})\hat{R}_{k-1} + d_{k-1}\left(\tilde{z}_k \tilde{z}^{\mathrm{T}} - H_{k,k-1} P_{k|k-1} H_{k,k-1}^{\mathrm{T}}\right) \tag{12}$$

where $d_k = (1-c)/(1-c^{k+1})$, c is the forgetting factor, $0.95 < c < 0.99$; $\tilde{z}_k = z_k - h(\hat{x}_{k|k-1})$ is the measurement innovation; and $H_{k,k-1}$ is the linearized observation matrix.

Designing Eq. (13) based on the EKF equations:

$$P_{xz,k|k-1} = P_{k|k-1} H_{k,k-1}^{\mathrm{T}} \tag{13}$$

Substituting $P_{k|k-1} = S_{k|k-1} S_{k|k-1}^{\mathrm{T}}$ into Eq. (13):

$$H_{k,k-1} = P_{xz,k|k-1}^{\mathrm{T}} / \left(S_{k|k-1}^{\mathrm{T}} S_{k|k-1}\right) \tag{14}$$

Substituting Eq. (13) and Eq. (14) into Eq. (12):

$$\hat{R}_k = (1 - d_{k-1})\hat{R}_{k-1} + d_{k-1} \left(\tilde{z}_k \tilde{z}^{\mathrm{T}} - P_{xz,k|k-1}^{\mathrm{T}} \left(S_{k|k-1}^{\mathrm{T}} S_{k|k-1}\right)^{-1} P_{xz,k|k-1}\right) \tag{15}$$

The specific steps of the IAHSRCKF algorithm are represented as:

i) System initialization [17]:

$$\begin{cases} \hat{x}_0 = E(x_0) \\ S_0 = \mathrm{chol}(p_0) \\ \hat{R}_0 = R_0 \end{cases} \tag{16}$$

where chol$(*)$ represents the Cholesky decomposition.

ii) Prediction process

(a) Calculating the higher-order cubature points ($i = 0, 1, ..., 2n^2$):

$$x_{i,k-1|k-1} = S_{k-1|k-1}\xi_i + \hat{x}_{k-1|k-1} \tag{17}$$

where $S_{k-1|k-1} = \mathrm{chol}(P_{k-1|k-1})$.

(b) Calculating the propagated cubature points:

$$x^*_{i,k|k-1} = f\left(x_{i,k|k-1}\right) \tag{18}$$

(c) Estimating the state prediction:

$$\hat{x}_{k|k-1} = \sum_{i=0}^{2n^2} \omega_i x^*_{i,k|k-1} \tag{19}$$

(d) Calculating the square-root of the predicted error covariance matrix:

$$S_{k|k-1} = \mathrm{qr}\begin{bmatrix} \sqrt{\omega_0}\left(x^*_{0,k|k-1} - \hat{x}_{k|k-1}\right) \cdots \\ \sqrt{\omega_{2n^2}}\left(x^*_{2n^2,k|k-1} - \hat{x}_{k|k-1}\right) \sqrt{Q_{k-1}} \end{bmatrix} \tag{20}$$

where qr$(*)$ represents the Q-R decomposition.

iii) Update process

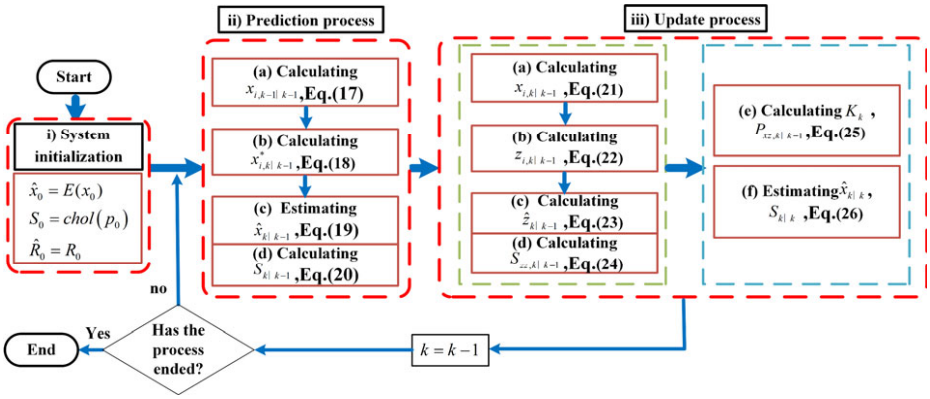

FIGURE 1. The flowchart of IAHSRCKF algorithm.

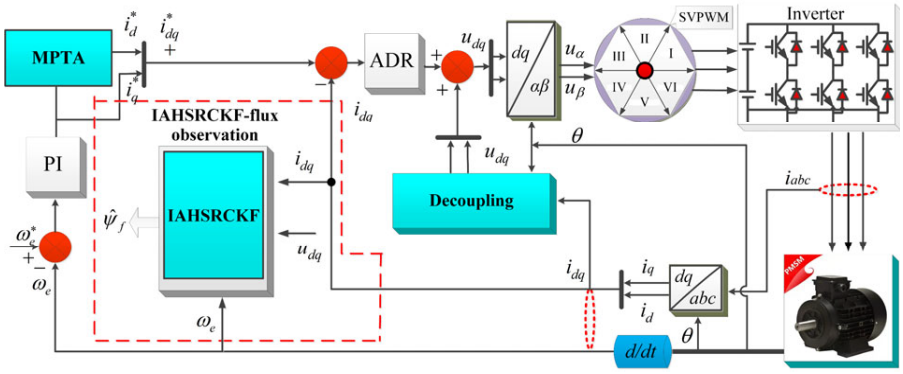

FIGURE 2. The control system diagram of PMSM.

(a) Calculating the higher-order cubature points ($i = 0, 1, ..., 2n^2$):

$$x_{i,k|k-1} = S_{k|k-1}\xi_i + \hat{x}_{k|k-1} \tag{21}$$

(b) Calculating the propagated cubature points:

$$z_{i,k|k-1} = h\left(x_{i,k|k-1}\right) \tag{22}$$

(c) Measurement prediction:

$$\hat{z}_{k|k-1} = \sum_{i=0}^{2n^2} \omega_i z_{i,k|k-1} \tag{23}$$

(d) Calculating the square root of the innovation covariance matrix:

$$S_{zz,k|k-1} = \mathrm{qr}\left[\begin{array}{c} \left[\sqrt{\omega_0}\left(z_{0,k|k-1} - \hat{z}_{k|k-1}\right)\cdots \right. \\ \left. \sqrt{\omega_{2n^2}}\left(z_{2n^2,k|k-1} - \hat{z}_{k|k-1}\right)\sqrt{\hat{R}_k} \right] \end{array}\right] \tag{24}$$

where $\sqrt{\hat{R}_k}$ is the Cholesky decomposition factor of matrix $\hat{R}_k$.

(e) Calculating the cross-covariance matrix and the gain matrix:

$$\begin{cases} P_{xz,k|k-1} = \sum_{i=0}^{2n^2} \omega_i \left[x_{i,k|k-1} - \hat{x}_{k|k-1}\right] \times \left[z_{i,k|k-1} - \hat{z}_{k|k-1}\right]^{\mathrm{T}} \\ K_k = \left[P_{xz,k|k-1}/S^{\mathrm{T}}_{zz,k|k-1}\right]/S_{zz,k|k-1} \end{cases} \tag{25}$$

(f) Estimating the state and the square-root of its covariance matrix:

$$\begin{cases} \hat{x}_{k|k} = \hat{x}_{k|k-1} + K_k\left[z_k - \hat{z}_{k|k-1}\right] \\ S_{k|k} = \mathrm{chol}^*\left[S_{k|k-1}, K_k S_{zz,k|k-1}, -1\right] \end{cases} \tag{26}$$

where chol* represents the Cholesky update.

After correcting the predicted value to obtain the optimal estimate of the system state variable $\hat{x}_{k|k}$ at time step k and the square root of its covariance matrix $S_{k|k}$, return to Eq. (17) for the next state cycle. Fig. 1 shows the flowchart of IAHSRCKF algorithm.

4. ANALYSIS OF SIMULATION RESULTS

To verify the effectiveness of the proposed algorithm, simulation experiments were conducted using MATLAB. Table 1 shows the PMSM parameters, and Fig. 2 presents the diagram of motor magnetic flux observation system. The specific experimental conditions are shown in Table 2.

Figures 3(a) and 3(b) show the comparison curves of flux linkage identification results for UKF, CKF, SRCKF, and IAHSRCKF. From Fig. 3, it can be observed that in the speed regulation conditions at 0 s and 2 s, the flux linkage values monitored by traditional UKF, CKF, and SRCKF exhibit significant overshoot. However, CKF and SRCKF converge faster than UKF, which requires some time to accurately track the changes

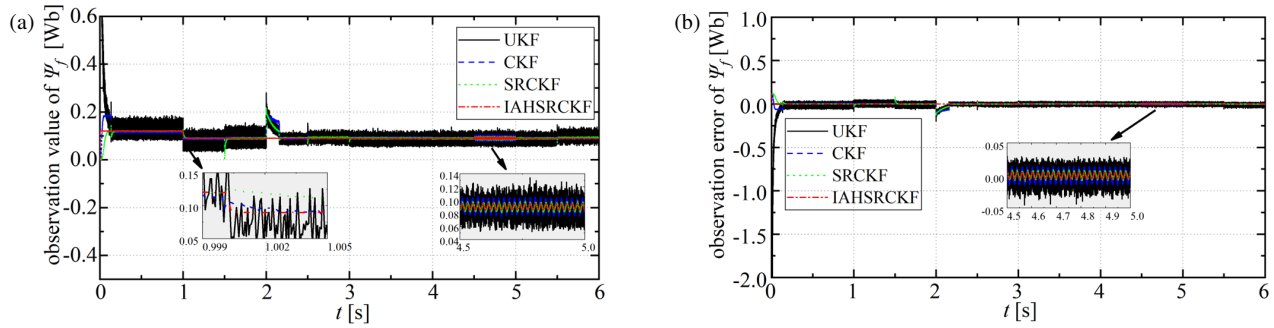

FIGURE 3. The comparison of flux identification results for UKF/CKF/SRCKF/IAHSRCKF. (a) Observation value of $\hat{\psi}_f$. (b) Observation error of $\hat{\psi}_f$.

TABLE 1. The nominal parameters of PMSM.

Motor parameters	Unit	Value
Rated voltage/u_{dc}	V	600
Rated speed/n_N	r/min	1900
Stator resistance/R_s	Ω	2.75
Number of pole pairs/n_p	pairs	2
d-axis inductance/L_d	H	0.004
q-axis inductance/L_q	H	0.009
Permanent-magnet flux linkage/ψ_f	Wb	0.12
Moment of inertia/J	kg·m^2	0.029

in flux linkage. In contrast, the IAHSRCKF not only avoids significant overshoot and oscillation but also provides high accuracy in tracking the flux linkage changes. When the PMSM's resistance, inductance, moment of inertia, and damping undergo perturbations, the flux linkage observed by UKF, CKF, and SRCKF exhibits considerable errors, and the tracking accuracy is poor. In comparison, IAHSRCKF accurately tracks the flux linkage with minimal error. At 1 s, when the PMSM flux linkage experiences a numerical perturbation, only IAHSRCKF demonstrates high-precision tracking performance, converging stably to 0.009. When time-varying disturbances are introduced at 4.5 s, the flux linkage observed by UKF, CKF, and SRCKF fluctuates significantly, and the error does not meet the high-accuracy observation requirements of the observer. In contrast, the IAHSRCKF algorithm accurately estimates the flux linkage changes, with minimal amplitude variation and greater stability.

In summary, compared with the other three Kalman algorithms, the IAHSRCKF algorithm, which combines fifth-order cubature integration with the square root and incorporates a time-varying noise statistical estimator, demonstrates stronger adaptability, and effectively overcomes filtering divergence. Therefore, it can accurately observe flux linkage during parameter perturbations. When external time-varying disturbances occur, the estimated curve exhibits minimal fluctuation, with excellent estimation accuracy and stronger adaptability.

5. ANALYSIS OF RT-LAB EXPERIMENTAL RESULTS

To further verify the effectiveness of this method, hardware-in-the-loop simulation (HILS) experiments of the PMSM drive

TABLE 2. The experimental conditions.

Time/s	Perturbation	range
0	n/r/min	0→1000
1.0	ψ_f/Wb	$0.12 \rightarrow 0.09$
1.5	R_s/Ω	$2.75 \rightarrow 3.85$
2.0	n/r/min	$1000 \rightarrow 2000$
2.5	L_q/H	$0.009 \rightarrow 0.006$
3.0	L_d/H	$0.004 \rightarrow 0.003$
3.5	J/kg·m^2	$0.029 \rightarrow 0.04$
4.0	B/N·m·s/rad	$0.001 \rightarrow 0.004$
4.5	T_L/N·m	$15 \rightarrow 15 + 2\sin 300t$
5.0	T_L/N·m	$15 + 2\sin 300t \rightarrow 15$
5.5	T_L/N·m	$15 \rightarrow 20$

system are implemented using RT-Lab. Fig. 4 shows the RT-Lab experimental platform, and Fig. 5 illustrates the RT-Lab experimental setup for UKF/ CKF /SRCKF/IAHSRCKF. The experimental operating conditions for the PMSM are identical to those used in the simulation, as detailed in Table 2. The simulation parameters are consistent with the experimental parameters.

A comparison between Fig. 3 and Fig. 5 shows that the results of the hardware-in-the-loop experiment are consistent with the simulation results. While the experimental results obtained from the RT-Lab platform exhibit lower precision than simulations, both the overall variation trends and numerical values

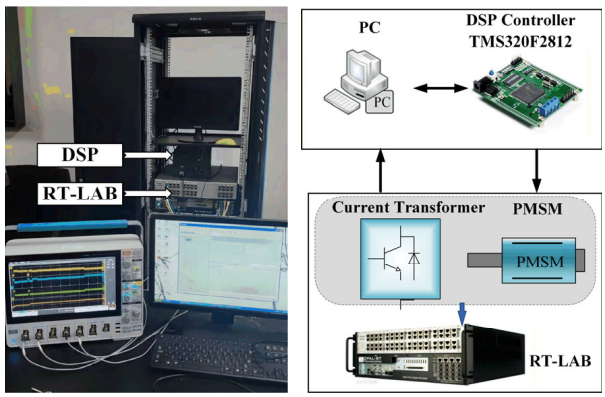

FIGURE 4. The experimental platform of RT-LAB.

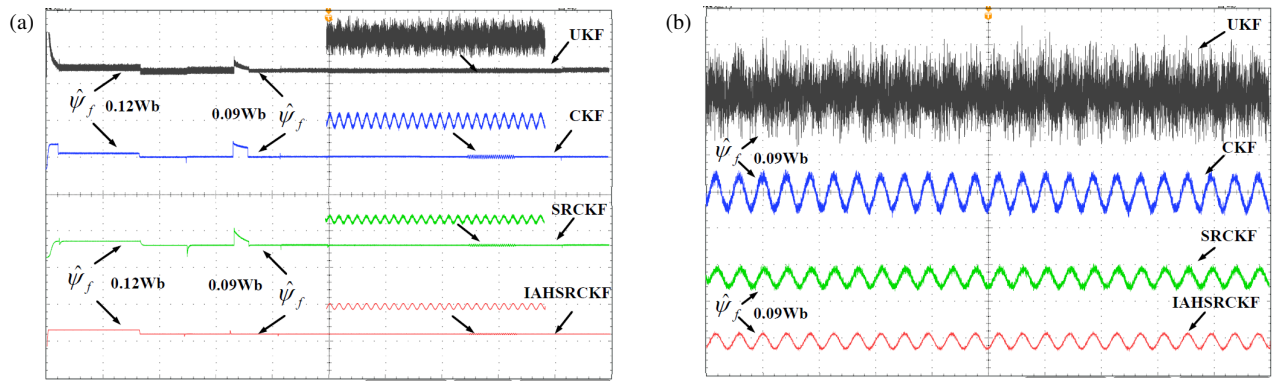

FIGURE 5. The experimental diagram of RT Lab. (a) The overall experimental results. (b) The amplification experiment results of 4.5 s–5 s.

of the curves remain consistent, effectively validating the operational performance under realistic motor conditions.

When comparing the four algorithms, the IAHSRCKF demonstrates accurate flux linkage tracking, stronger adaptability, and effectively overcomes filtering divergence. It calculates the permanent magnet flux linkage accurately, is less affected by motor parameters and external disturbances, and exhibits strong robustness.

6. CONCLUSION

In this paper, an online monitoring method for the permanent-magnet flux linkage in PMSM is proposed, based on an improved adaptive higher-order square-root cubature Kalman flux-linkage observer. The proposed method integrates fifth-order cubature integration and an adaptive estimator with the square-root cubature Kalman filter, enabling real-time monitoring of the PMSM's permanent-magnet flux linkage. Both simulated and experimental results demonstrate that the proposed method features a simple structure, accurately calculates the permanent-magnet flux linkage, and exhibits minimal susceptibility to motor parameter variations and external disturbances. Moreover, the method showcases strong robustness, making it a promising solution for accurate flux linkage estimation in practical applications.

ACKNOWLEDGEMENT

This work was supported by the Postgraduate Scientific Research Innovation Project of Hunan Province Grant CX20231107.

REFERENCES

[1] Liu, J., Y. Yang, X. Li, K. Zhao, Z. Yi, and Z. Xin, "Improved model-free continuous super-twisting non-singular fast terminal sliding mode control of IPMSM," *IEEE Access*, Vol. 11, 85 361–85 373, 2023.

[2] Yi, Z., X. Li, Y. Yin, J. Liu, and K. Zhao, "Deep flux weakening control of IPMSM based on d-axis current error integral regulator," *Progress In Electromagnetics Research M*, Vol. 118, 163–175, 2023.

[3] He, Y., K. Zhao, Z. Yi, and Y. Huang, "Improved terminal sliding mode control of PMSM dual-inertia system with acceleration feedback based on finite-time ESO," *Progress In Electromagnetics Research M*, Vol. 134, 21–30, 2025.

[4] Xiao, Q., Z. Wang, X. Wei, Y. Yang, Y. Zhang, and Z. Cheng, "Double closed-loop model-free super-twisting terminal sliding mode control algorithm of IPMSM based on third-order super-twisting observer," *Progress In Electromagnetics Research C*, Vol. 149, 47–58, 2024.

[5] Liu, J., Z. Wang, F. Deng, K. Zhao, and X. Li, "Continuous high-order sliding mode optimization control of PMSM based on STSMO," *Progress In Electromagnetics Research Letters*, Vol. 127, 29–37, 2025.

[6] Li, X., J. Liu, Y. Yin, and K. Zhao, "Improved super-twisting non-singular fast terminal sliding mode control of interior permanent magnet synchronous motor considering time-varying disturbance of the system," *IEEE Access*, Vol. 11, 17 485–17 496, 2023.

[7] Wang, J., R. Zhou, and J. Liu, "New non-singular fast terminal sliding mode control of permanent magnet synchronous motor based on super-twisting sliding mode observer," *Progress In Electromagnetics Research C*, Vol. 146, 151–162, 2024.

[8] Mu, Y., X. Li, and X. Chen, "Permanent magnet flux linkage observation for PMSM based on adaptive high-order sliding mode," *Journal of Electronic Measurement and Instrumentation*, Vol. 34, No. 3, 163–170, 2020.

[9] Zhang, J. and R. Han, "An improved permanent magnet magnetic link observation algorithm for adaptive permanent magnet synchronous motor," *Journal of Taiyuan University of Science and Technology*, Vol. 42, No. 1, 26–31, 2021.

[10] Yan, J., S. Liu, X. Wu, *et al.*, "Online magnet flux linkage identification of PMSM based on position triangular signal injection," *Proceedings of the CSEE*, Vol. 39, No. 3, 845–856, 2019.

[11] Wang, T., A. Y. Wang, Y. X. Jin, and J. Sun, "Research on fault-tolerant control method for demagnetization faults of permanent magnet synchronous motor," in *2018 IEEE Student Conference on Electric Machines and Systems*, 1–6, Huzhou, China, 2018.

[12] Zhao, K., J. She, C. Zhang, J. He, G. Huang, and J. Liu, "Robust closed-loop torque control for PMSM of railway traction considering demagnetization," in *IECON 2019 — 45th Annual Conference of the IEEE Industrial Electronics Society*, Vol. 1, 6916–6921, Lisbon, Portugal, 2019.

[13] Shi, Y., K. Sun, H. Ma, *et al.*, "Online identification of permanent magnet flux linkage for interior permanent magnet synchronous motor," *Transactions of China Electrotechnical Society*, Vol. 26,

No. 9, 48–53, 2011.

[14] Fang, B., W. Li, D. Chen, K. Zhao, Q. Zhang, and H. Liu, "Parameter identification of permanent magnet synchronous motors based on multi-innovation recursive least squares and multi-innovation extended Kalman filter algorithms," *Journal of Shanghai Jiao Tong University*, 2025.

[15] Li, X., J. Liu, K. Zhao, Y. Yin, and L. Zou, "An improved model-free sliding mode control algorithm of super-twisting for SPMSM," *Progress In Electromagnetics Research C*, Vol. 135, 195–210, 2023.

[16] Zhang, R. Y., C. S. Zheng, P. C. Shi, L. F. Zhao, C. F. Gong, and C. L. Zhou, "Sensorless control of PMSM based on improved PSO and generalized fifth order CKF algorithm," *Electric Machines and Control*, Vol. 25, No. 7, 120–128, 2021.

[17] Li, X., J. Liu, K. Zhao, Y. Yin, and L. Zou, "Improved non-singular fast terminal sensor-less sliding mode control of IPMSM considering external disturbance and parameter perturbation," *Progress In Electromagnetics Research B*, Vol. 102, 81–98, 2023.